

Subsurface ocean warming preceded Heinrich Events

Lars Max ¹✉, Dirk Nürnberg ², Cristiano M. Chiessi ³, Marlene M. Lenz ⁴ & Stefan Mulitza ¹

Although the global environmental impact of Laurentide Ice-Sheet destabilizations on glacial climate during Heinrich Events is well-documented, the mechanism driving these ice-sheet instabilities remains elusive. Here we report foraminifera-based subsurface (~150 m water depth) ocean temperature and salinity reconstructions from a sediment core collected in the western subpolar North Atlantic, showing a consistent pattern of rapid subsurface ocean warming preceding the transition into each Heinrich Event identified in the same core of the last 27,000 years. These results provide the first solid evidence for the massive accumulation of ocean heat near the critical depth to trigger melting of marine-terminating portions of the Laurentide Ice Sheet around Labrador Sea followed by Heinrich Events. The repeated build-up of a subsurface heat reservoir in the subpolar Atlantic closely corresponds to times of weakened Atlantic Meridional Overturning Circulation, indicating a precursor role of ocean circulation changes for initiating abrupt ice-sheet instabilities during Heinrich Events. We infer that a weaker ocean circulation in future may result in accelerated interior-ocean warming of the subpolar Atlantic, which could be critical for the stability of modern, marine-terminating Arctic glaciers and the freshwater budget of the North Atlantic.

¹MARUM—Center for Marine Environmental Sciences, University of Bremen, Bremen 28359, Germany. ²GEOMAR, Helmholtz Centre for Ocean Research Kiel, Kiel 24148, Germany. ³School of Arts, Sciences and Humanities, University of São Paulo, São Paulo, Brazil. ⁴Institute of Geology and Mineralogy, University of Cologne, Cologne 50674, Germany. ✉email: lmax@marum.de

The deposition of ice-rafted debris layers in the glacial North Atlantic (known as Heinrich Events) provides evidence for a substantial freshwater release via melting icebergs in response to past instabilities of the Laurentide Ice Sheet (LIS)^{1–3}. Although the impact of Heinrich Events on global climate has been studied thoroughly during the last decades^{4–6}, the driving mechanism behind the episodic iceberg-discharge during Heinrich Events is a matter of ongoing debate^{7–10}. A commonly discussed hypothesis is that Heinrich Events were initiated by the periodic unstable flow of the LIS, controlled by internal ice-sheet oscillations under otherwise stable environmental conditions, known as “binge-purge” hypothesis⁷. It is assumed that the massive freshwater release during Heinrich Events initiated strong disruptions of the Atlantic Meridional Overturning Circulation (AMOC)³ and surface-ocean cooling of the North Atlantic⁴. However, surface ocean temperature and ice-rafted debris (IRD) proxy data from the high latitudes of the North Atlantic indicate that surface-ocean cooling occurred hundreds to thousands of years earlier than ice-rafting events in the North Atlantic¹⁰. Moreover, proxy data of AMOC strength show that deep ocean-circulation weakened prior to Heinrich Events in the North Atlantic⁶. Other studies propose a strong impact of weaker overturning circulation on LIS dynamics and the onset of Heinrich Events^{9,11–13}. Based on numerical modelling simulations, a reduced AMOC would lead to strong subsurface warming and rapid retreat of ice-shelves around the Labrador Sea that is followed by the destabilization of the LIS during Heinrich Events^{9,13}. Proxy data of bottom-water temperatures show that the mid-depth North Atlantic indeed warmed prior to Heinrich Events and thus seem to support this mechanism¹⁴. Nevertheless, proxy records reflecting subsurface ocean temperature variability near the Labrador Sea, close to the grounding line of marine-based portions of the LIS, are not available yet, hampering the evaluation of subsurface ocean warming as the trigger of Heinrich Events.

We studied fluctuations in subsurface ocean conditions relative to the occurrence of Heinrich Events at a site located to the east of Newfoundland in the subpolar western North Atlantic (marine sediment core GeoB18530-1; 42° 50' N, 49° 14' W, 1888 m water depth; Fig. 1a) at high temporal resolution (~250 years on average) over the last 27,000 years. We analysed the Mg/Ca ratio of subsurface dwelling planktonic foraminifera *Neogloboquadrina pachyderma* sinistral (*N. pachyderma* sin.) as a proxy for subsurface temperatures (subSST_{Mg/Ca} at ~150 m water depth) from site GeoB18530-1 (see “Methods” and Supplementary Figs. 1–3). Combined information from subSST_{Mg/Ca} data and the stable oxygen isotopic composition ($\delta^{18}\text{O}$) of *N. pachyderma* sin. allow calculating the regional ice-volume-corrected oxygen isotopic composition of seawater ($\delta^{18}\text{O}_{\text{ivc-sw}}$) as a proxy for salinity (see “Methods”). The chronostratigraphy of sediment core GeoB18530-1 is based on 20 accelerator mass spectrometer ¹⁴C ages spanning the last 35,000 years (Supplementary Fig. 4 and Supplementary Table 1). Site GeoB18530-1 is located at the southern boundary of the North Atlantic Subpolar Gyre (Fig. 1a). Today this location is under the influence of warm and saline waters of the North Atlantic Current (NAC), which is an integral part of the upper branch of the AMOC. Observational and modelling data show that modern inter-annual to decadal variability of temperature and salinity in the study area is controlled by Subpolar Gyre dynamics¹⁵, suggesting that site GeoB18530-1 is a sensitive recorder of changes in ocean temperature and salinity. Sediment core GeoB18530-1 is ideally located to investigate the relative timing of past ocean dynamics in temperature and salinity against Heinrich Events associated with LIS instabilities within Hudson Strait because of: (i) its location close to the exit of the Labrador Sea within the IRD-belt¹⁶, the North Atlantic gateway of the main iceberg trajectory associated with Heinrich Events (Fig. 1b); (ii) the well-defined IRD layers deposited during Heinrich Events (Fig. 2a); and (iii) the fact that all proxy records were established from the same

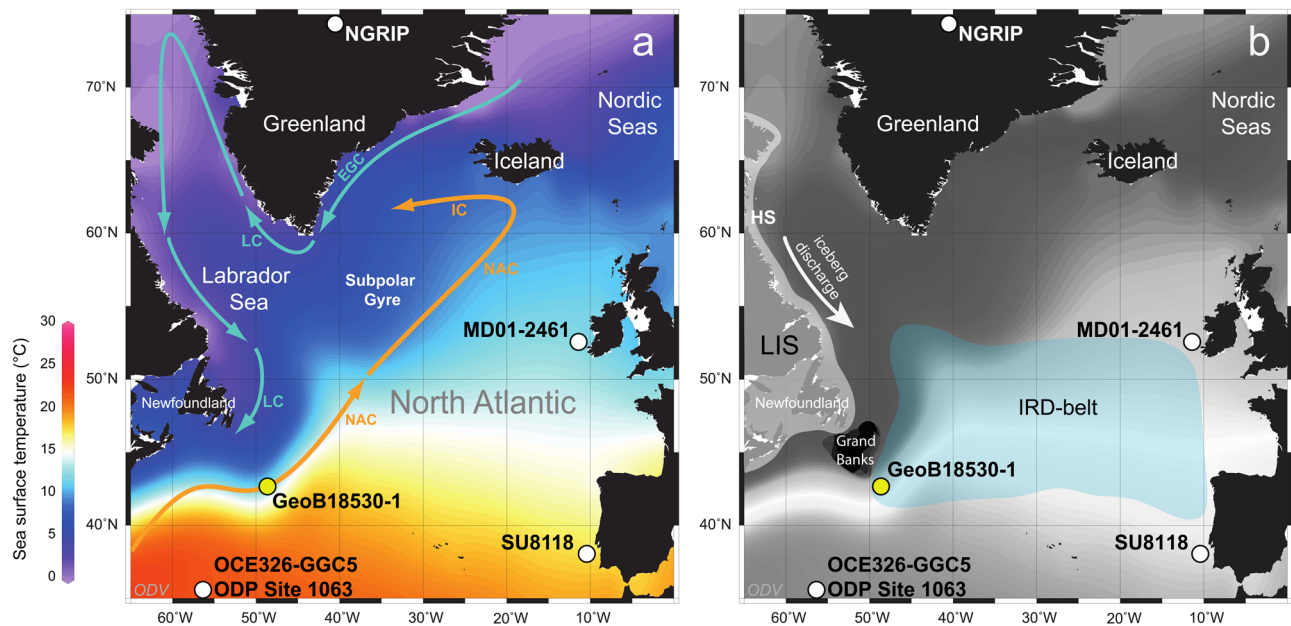


Fig. 1 Modern surface-ocean conditions in the North Atlantic, the extension of the Laurentide Ice Sheet (LIS) and the IRD-belt in the North Atlantic during the Last Glacial Maximum. **(a)** Annual mean sea surface temperature²⁰ (colour shading) and surface circulation¹⁵ (arrows) in the study area. Yellow dot: location of core site GeoB18530-1 (42° 50' N, 49° 14' W; 1,888 m water depth; this study); white dots: location of reference core sites MD01-2461 (51°45' N, 12° 55' W; 1153 m water depth), SU8118 (37° 46' N, 10°11' W; 3135 m water depth), OCE326-GGC5/ODP Site 1063 (33° 42' N, 57° 35' W; 4550 m water depth), and North Greenland Ice Core Project (NGRIP; 75° 5' N, 42° 17' W). EGC East Greenland Current, IC Irminger Current, LC Labrador Current, NAC North Atlantic Current. **(b)** Area shaded in white: LIS extent⁵³; area shaded in green: IRD-belt in the North Atlantic¹⁶; HS Hudson Strait. This map was generated with Ocean Data View⁵⁴.

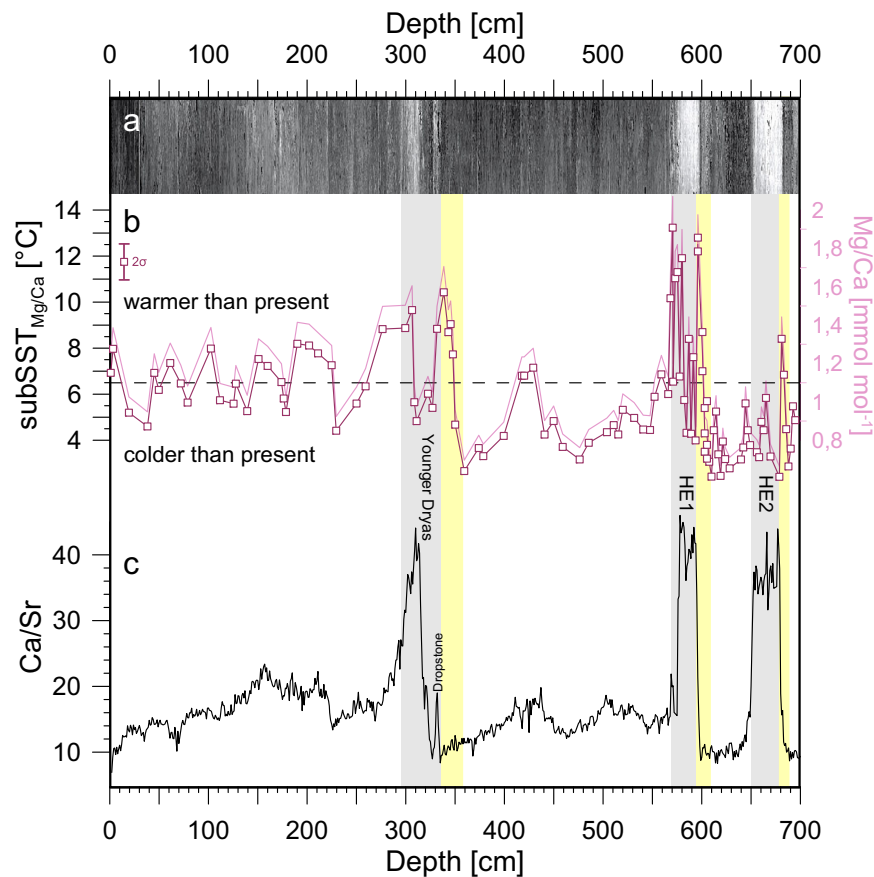


Fig. 2 Proxy records from sediment core GeoB18530-1 versus core depth in comparison to digital core image. **a** High-resolution digital core image¹⁷. **b** Foraminiferal $Mg/Ca_{N. pachyderma\ sin.}$ ratios and calculated subsurface temperatures ($subSST_{Mg/Ca}$) with analytical uncertainty (2σ). **c** X-ray fluorescence scanning-derived calcium to strontium ratios (Ca/Sr). yellow bars = phases of increases in $subSST_{Mg/Ca}$ into Heinrich Events and the Younger Dryas; grey bars = Heinrich Layers (HE2 = Heinrich Event 2, HE1 = Heinrich Event 1) and the Younger Dryas. Dashed horizontal line in Fig. 1b indicates modern temperature at ~150 m water depth close to site GeoB18530-1²⁰.

sediment core allowing robust determination of past ocean–ice-sheet interactions without temporal offsets and independent of any age modelling issues.

Results

Subsurface ocean warming prior to Heinrich Events. The most intriguing finding in our records is a recurring pattern of massive rises of $subSST_{Mg/Ca}$ in the subpolar western North Atlantic (Fig. 2b). Another salient feature is the presence of very well-preserved IRD layers at site GeoB18530-1¹⁷ (Fig. 2a). To further characterize the IRD layers we used the elemental ratio of calcium to strontium (Ca/Sr) from bulk sediments of core GeoB18530-1 as a proxy for detrital carbonate associated with Heinrich Event 1 and 2^{2,18,19} (see “Methods”). The IRD layers are characterized by elevated Ca/Sr ratios as expected from the high content of detrital carbonate originating from Paleozoic limestone and dolostone from Hudson Bay and Hudson Strait² (Fig. 2c). Remarkably, the onset of subsurface ocean warmings clearly precedes the deposition of Heinrich Layers by several centimetres with respect to core depth (Fig. 2). It is important to note that the timing of $subSST_{Mg/Ca}$ increases prior to Heinrich Events is systematic and independent of any age model uncertainties. A closer look reveals that warmest subsurface ocean temperatures appear synchronous to the onset of IRD deposition during Heinrich Events (Fig. 2b). The timing of the $subSST_{Mg/Ca}$ warming peaks is further constrained by radiocarbon ages, suggesting a calibrated median age of ~17.1 ka BP at the beginning of Heinrich Event 1 and a

calibrated median age of ~25.4 ka BP close to the warming peak prior to Heinrich Event 2 (Supplementary Table 1). Subsurface temperatures rise to 8.4 °C and 12.5 °C at the onset of IRD layers of Heinrich Events 2 and 1, respectively (Fig. 2b, c). Modern hydrographic data close to site GeoB18530-1²⁰ exhibit a subsurface ocean temperature of ~7 °C for the inferred habitat depth range of *N. pachyderma sin.* (see Supplementary Fig. 3).

After the onset of Heinrich Events, subsurface waters experienced a phase of rapid cooling and freshening (Fig. 3). At this point, the cooling and freshening signals describe the well-known response to massive meltwater intrusions in the subpolar North Atlantic during Heinrich Events². A second rise in temperature and salinity is evident at the later phase of Heinrich Events, most pronounced during Heinrich Event 1 (Fig. 3). This is consistent with findings derived from Heinrich layers of the central North Atlantic showing that Heinrich Event 1 is subdivided into an early phase (Heinrich Event 1.1; 17.1–15.5 ka BP) and a late phase (Heinrich Event 1.2; 15.9–14.3 ka BP) of IRD deposition, interpreted as two different ice-stream advances²¹. In particular, the synchronous onset of marked IRD deposition when $subSST_{Mg/Ca}$ appears to be warmest provides strong evidence for a causal role of subsurface ocean temperatures in triggering Heinrich Events of the last 27,000 years (Fig. 3).

Subsurface ocean warming linked to AMOC slowdowns. Further comparison of proxy records of North Atlantic–North

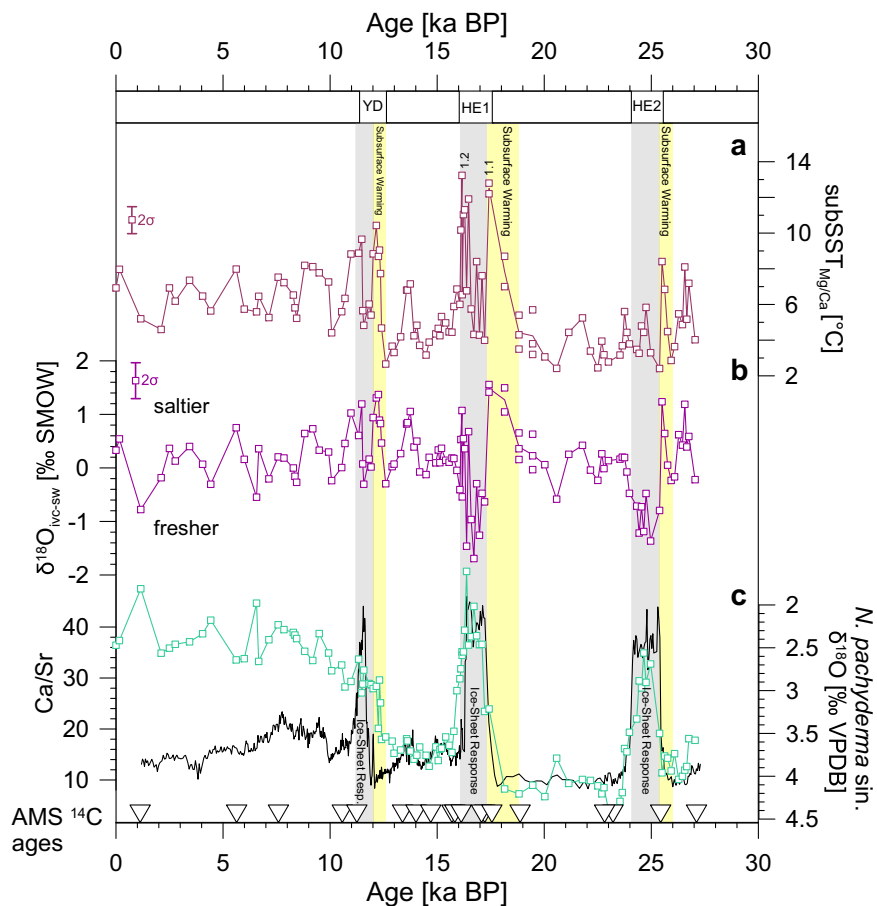


Fig. 3 Subsurface ocean variability and Heinrich Events over the last 27,000 years from sediment core GeoB18530-1. **a** Subsurface temperatures (subSST_{Mg/Ca}) with analytical uncertainty (2σ). **b** Ice-volume-corrected oxygen isotopic composition of seawater ($\delta^{18}\text{O}_{\text{IVC-sw}}$) with analytical uncertainty (2σ). **c** Oxygen isotope composition ($\delta^{18}\text{O}$) of *Neogloboquadrina pachyderma sinistral* and X-ray fluorescence scanning-derived element ratio of calcium to strontium (Ca/Sr). Bottom: Open triangles indicate calibrated radiocarbon ages (AMS ^{14}C ages). yellow bars = phases of increases in subSST_{Mg/Ca} into Heinrich Events and the Younger Dryas (YD); grey bars = Heinrich Layers (HE2 Heinrich Event 2, HE1 Heinrich Event 1 with Heinrich Event 1.1 and Heinrich Event 1.2 indicated)²¹ and YD.

Greenland Ice Core Project (NGRIP) temperature variability and AMOC strength yields three key observations (Fig. 4). First, pronounced temperature increases prior to Heinrich Events are neither visible in the NGRIP^{22,23} record of atmospheric temperatures, nor in North Atlantic sea surface temperatures⁴ over the last 27,000 years (Fig. 4a, e). Moreover, North Atlantic sea surface temperatures cool (warm) when subSST_{Mg/Ca} warm (cool). The opposing temperature trends are particularly evident prior to Heinrich Events as well as the Younger Dryas and we conclude that subsurface water masses must be very well isolated from the surface ocean of the subpolar Atlantic during these intervals (Fig. 4b, e).

Second, early subsurface ocean warming is also evident from site MD01-2461 located in the subpolar eastern North Atlantic, being most pronounced prior to Heinrich Event 1²⁴ (Fig. 4d). The correlation with elevated IRD flux at the same site is supposed to reflect a situation, in which anomalously warm conditions in the subpolar eastern North Atlantic caused ablation of the marine ice-margin of the British Ice Sheet²⁴. This is in line with palaeoglaciological studies describing a significant ice-margin retreat of the British-Irish Ice Sheet between ~19 and 17 ka BP associated with catastrophic disintegration of the North Sea ice-bridge and an enormous outburst from a meltwater lake into the southern North Sea²⁵. Based on the close correspondence of subSST_{Mg/Ca} increases at both margins of the subpolar North

Atlantic (Fig. 1), we hypothesize that a large volume of heat was stored in the interior of the subpolar North Atlantic prior to Heinrich Event 1. Our interpretation is in line with previous findings from benthic Mg/Ca bottom water temperature reconstructions of the mid-depth Northwest Atlantic proposing significant warming of the interior-ocean prior to Heinrich Events¹⁴.

Third, proxy data of AMOC variability^{6,26} show that deep-ocean circulation weakened during Heinrich Stadial 2 and 1, preceding Heinrich Events by 1–2 kyrs¹⁴ (Fig. 4f). The signal of an early decline in AMOC preceding Heinrich Events by 1–2 kyrs exceeding the typical range of age model uncertainties for paleo-reconstructions of several hundreds of years and seems to be quite robust. Our subSST_{Mg/Ca} record indicates the build-up of ocean heat in the subpolar western North Atlantic during Heinrich Stadials and the Younger Dryas (Fig. 4b). Accordingly, we found calibrated mean ages for the beginning of subsurface ocean warming of ~25.9 ka BP during Heinrich Stadial 2, ~18.6 ka BP at the transition to Heinrich Stadial 1 and ~12.5 ka BP at the beginning of the Younger Dryas, during repeated slowdowns of the AMOC. These results point to a close temporal relationship between weaker overturning circulation and the increase in ocean heat content in the subpolar western North Atlantic (Fig. 4b, f). However, we found a delay in IRD deposition towards the end of the Younger Dryas interval at site GeoB18530-1 (Fig. 4b, c). This

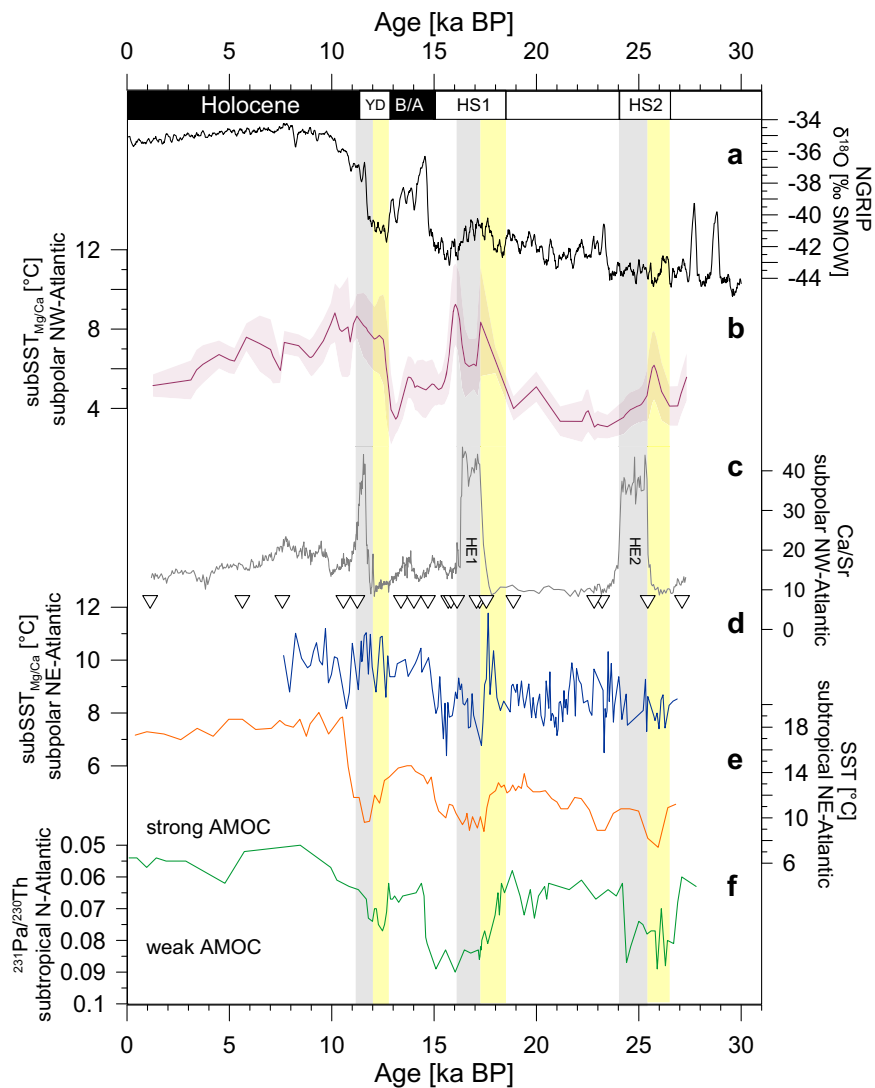


Fig. 4 Comparison of proxy records from sediment core GeoB18530-1 to representative Greenland- North Atlantic proxy records over the last 27,000 years. **a** North Greenland Ice Core Project (NGRIP)^{22,23} stable oxygen isotopic composition ($\delta^{18}\text{O}$) reflecting atmospheric temperatures over Greenland. **b** Mean ages from age model ensemble for subsurface temperatures of core GeoB18530-1 with 95% confidence interval (this study). **c** X-ray fluorescence scanning-derived calcium to strontium ratios (Ca/Sr) (grey line) and age control points derived from calibrated AMS ^{14}C ages (open triangles) from core GeoB18530-1 (this study). **d** Subsurface temperatures from core MD01-2461 (eastern subpolar North Atlantic)²⁴. **e** Alkenone sea surface temperatures from core SU8118 (eastern subtropical North Atlantic)⁴. **f** Pa/Th ratio reflecting the strength of the Atlantic Meridional Overturning Circulation (AMOC). Time series from 0 to 19 ka BP derived from core OCE326-GGC56⁶, time series from 20 to 27 ka BP derived from ODP Site 1063²⁶. Yellow bars = phases of increases in subSST_{Mg/Ca} into Heinrich Events and the Younger Dryas (YD); grey bars = Heinrich Layers (HE2 Heinrich Event 2, HE1 Heinrich Event 1) and the YD. B/A Bølling-Allerød interstadial, HS Heinrich Stadials.

difference may stem from the fact that the Younger Dryas is not a typical Heinrich Event with only modest and non-linear freshwater forcing (and modest AMOC weakening), proposed to be delivered to the ocean via, e.g., the St. Lawrence River²⁷ or Mackenzie River²⁸.

The rapid North Atlantic subsurface ocean warming during AMOC weakening is a feedback mechanism observed in several numerical modelling simulations^{29–31}. As soon as the AMOC is weakened, due to freshwater hosing, immediate cooling and isolation of the surface ocean from subsurface waters is observed in the models^{29–31}. Physically, reduced convection of North Atlantic Deep Water leads to a redistribution of heat in the Atlantic basin and the interior-ocean warms, in particular in the equatorial- and South Atlantic²⁹. Notably, some models exhibit ocean warming in the Atlantic basin down to ~2500 m water depth within decades after AMOC slowdown^{30,31}. At the same

time, subsurface advection of warm waters by the subtropical and subpolar gyres are important for the poleward heat transport to the North Atlantic. As long as deep-water convection weakens in the North Atlantic, the surface ocean cools in the subpolar Atlantic. The subsurface ocean further warms because of the background energy transport of the gyre system together with strong isolation from freshening of the surface ocean, thereby creating a growing temperature inversion³¹. The magnitude of interior-ocean warming strongly depends on the used model, as well as on model configurations and varies between 4 and 6 °C^{30,31}, consistent with our subSST_{Mg/Ca} reconstructions. Moreover, as soon as the AMOC recovers from freshwater forcing with active deep convection in the North Atlantic, the surface ocean becomes warmer and interior-ocean temperatures become cooler due to invigorated AMOC³¹. Our records verify and expand results from theoretical modelling experiments^{29–31}, and we

propose subsurface ocean warming of the western subpolar North Atlantic is a natural feedback mechanism to slowdowns of the AMOC over the last 27,000 years.

Subsurface ocean warming as trigger for Heinrich Events.

Several ice-sheet modelling studies propose North Atlantic subsurface warming as a trigger for increased ice-rafting^{9,11–13,32}. Accordingly, the build-up of ocean heat near the grounding line of ice-shelves is a critical value in some of these models to trigger a rapid retreat of the ice-margin around the Labrador Sea^{9,13,32}. With continuous subsurface ocean warming the ice-shelf shrinks and accelerates the ice flow at the grounded line, triggering the rapid surge of the grounded ice and a massive iceberg discharge in the modelling simulations¹³. A more recent ice-sheet modelling study showed that without an ice-shelf relatively small fluctuations in subSST_{Mg/Ca} near Hudson Strait are sufficient to trigger Heinrich Events¹¹. Our findings are in close agreement with ice-sheet modelling studies, providing first solid evidence for subsurface ocean warming in the western subpolar North Atlantic as the trigger for ice-sheet instabilities during Heinrich Events^{9,11–13,32}.

Future AMOC slowdown and the build-up of ocean heat in the subpolar Atlantic. Instrumental time-series show a long-term increase in the North Atlantic heat content since the early 1950s and a close relationship to the accelerated mass loss of the Greenland Ice Sheet^{33–35}. However, it is yet unclear how AMOC variability contributes to the observed changes because of analytical limitations from relatively short instrumental time-series. The most recent report of the Intergovernmental Panel on Climate Change projects a future decline of the AMOC due to anthropogenic warming in the 21st century³⁶. New empirical data suggest the AMOC has been evolved to a point close to a critical transition to its weak circulation mode³⁷. Our findings suggest that past critical transitions to a weak AMOC mode are accompanied by the massive build-up of ocean heat in the western subpolar North Atlantic triggering ice-sheet instabilities during Heinrich Events. The projected weakening of the AMOC in the 21st century³⁶ may result in an amplified increase in the interior-ocean heat content that could be critical for the stability of modern, marine-terminating Arctic glaciers and the freshwater budget of the North Atlantic.

Methods

Mg/Ca and $\delta^{18}\text{O}$ measurements. For Mg/Ca analyses, ~100 individuals of the foraminiferal species *N. pachyderma* sin. were picked from sieved sediment samples of the size fraction >250 μm . Prior to geochemical analyses, the foraminiferal tests were opened gently between glass plates and samples split into one third for stable isotope analyses and two third for Mg/Ca measurements. Additional cleaning of each sample was done according to ref. 38. Mg/Ca analyses were performed with an axial-viewing ICP-OES Varian 720 ES (Inductively Coupled Plasma Optical Emission Spectrometry) at GEOMAR, Helmholtz-Centre for Ocean Research in Kiel. The levels of detection typically vary for each cation, ranging from 0.001 to 0.1 $\mu\text{g}/\text{ml}$. Mg/Ca was normalized to the ECRM 752–1 standard (3.761 mmol/mol Mg/Ca; according to ref. 39) and drift-corrected. Regular analyses of the ECRM 752–1 standard yield an analytical error of ± 0.01 mmol/mol for Mg/Ca.

Simultaneous measurements of Fe and Al were performed to monitor possible silicate contamination³⁸. Six out of 110 samples showed elevated Al/Ca values (>0.2 mmol/mol), however, are inconspicuous in the Mg/Ca value compared to neighbouring Mg/Ca values with no sign of potential contamination (Supplementary Fig. 1a). We identified one sample with an extremely high Al/Ca value of ~1.2 mmol/mol. A replicate measurement of this sample showed a very low Al/Ca value of ~0.04 mmol/mol, no sign of contamination, and nearly identical Mg/Ca values (1.93 mmol/mol with elevated Al/Ca value; 2.01 with low Al/Ca value). Obviously, the elevated Al/Ca values do not largely afflict the Mg/Ca values in the sample. A cross-plot of Mg/Ca values versus Al/Ca values further confirms the generally weak correlation between Mg/Ca and Al/Ca ($r^2 = \sim 0.14$; Supplementary Fig. 1b). Consequently, we decided to report all values. We note that discarding the six values with elevated Al/Ca values would not change the observed trends in the discussed time-series (Supplementary Fig. 1a).

Stable isotopes ($\delta^{18}\text{O}$) of *N. pachyderma* sin. were measured with Thermo Scientific MAT 253 mass spectrometers equipped with an automated Kiel IV Carbonate Preparation Device at MARUM, University of Bremen and at GEOMAR, Helmholtz-Centre for Ocean Research in Kiel. The $\delta^{18}\text{O}$ isotope values were calibrated versus the NBS19 (National Bureau of standards) carbonate standard and an in-house standard (“Standard Bremen”). The long-term analytical precision is 0.06‰ for $\delta^{18}\text{O}$. Results were calibrated to the VPDB scale, given in per mille (‰) relative to the VPDB.

Mg/Ca temperatures of *N. pachyderma* sin. The foraminiferal Mg/Ca ratios were converted into water temperatures considering different species-specific calibrations for *N. pachyderma* sin.:

$$\text{Mg/Ca}(\text{mmol/mol}) = 0.474 \exp(0.107 * T) \quad (1)$$

$$\text{Mg/Ca}(\text{mmol/mol}) = 0.13(\pm 0.037) * T(\text{degC}) + 0.35(\pm 0.17) \quad (2)$$

$$\text{Mg/Ca}(\text{mmol/mol}) = 0.4 * \exp(0.1 * T) \quad (3)$$

Comparison of converted core-top Mg/Ca temperature to instrumental temperatures²⁰ allowed assessment of the most suitable calibration for our study site (Supplementary Fig. 2). Assuming a mean habitat depth of 150 m for subsurface dwelling species of *N. pachyderma* sin.⁴⁰ yields a difference of 1.2 °C after calibration to Eq. 1 (ref. 41), 0.18 °C after calibration to Eq. 2 (ref. 42) and 4.32 °C after calibration to Eq. 3 (ref. 43). Consequently, we considered the calibration after ref. 42 as appropriate to convert the Mg/Ca ratio to subsurface temperatures.

Sensitivity of *N. pachyderma* sin. derived Mg/Ca signal to changes in habitat depth. A range of habitat depths from ~50 to 200 m has been reported for *N. pachyderma* sin.^{40,42}. Consequently, we checked whether changes in the assumed habitat depth may afflict the robustness of our results. To do so, we calculated the temperature gradient between 50 and 200 m water depth (ΔT_{200-50}) using modern instrumental data²⁰ from a water column profile near-site GeoB18530-1 (Supplementary Fig. 3). The ΔT_{200-50} is 2.05 °C, assuming a maximum shift in the habitat depth of *N. pachyderma* sin. in September. Given the large subsurface temperature amplitudes of up to 6 °C observed in our time series we conclude that only a small part of the total variability is explained by changes in the habitat depth.

Sensitivity of *N. pachyderma* sin. derived Mg/Ca to changes in the seasonal cycle. We further investigated the effect of major shifts in the seasonal cycle of *N. pachyderma* sin. on reconstructed subsurface temperatures. A study combining sediment trap data and modelling results suggests that the seasonality in the production of *N. pachyderma* sin. may have changed by up to 6 months between the Last Glacial Maximum (LGM) and full Heinrich conditions in the western subpolar North Atlantic⁴⁴. However, we note that reconstructed subsurface ocean warmings preceding Heinrich Events in our time series and thus, do not reflect full Heinrich conditions. Nevertheless, we investigated the effect of a possible change in seasonality assuming a maximum shift in seasonality from April to September, considering modern hydrographic data²⁰. The difference in subSST_{150m} between April (7.2 °C) and September (7.45 °C) is 0.25 °C at our core site (see Supplementary Fig. 3). We conclude that the effect of a seasonal shift in production of *N. pachyderma* sin. is minor on reconstructed subsurface temperatures.

Oxygen isotopic composition of seawater ($\delta^{18}\text{O}_{\text{sw}}$). We calculated the regional ice-volume-corrected $\delta^{18}\text{O}_{\text{sw}}$ record ($\delta^{18}\text{O}_{\text{sw, ivo}}$) considering changes in global $\delta^{18}\text{O}_{\text{sw}}$ due to continental ice-volume variability using the relative sea-level curve of ref. 45. To remove the temperature effect from the $\delta^{18}\text{O}_{\text{sw, ivo}}$ record we applied the temperature versus $\delta^{18}\text{O}_{\text{calcite}}$ equation of ref. 46:

$$\delta^{18}\text{O}_{\text{calcite}}(\text{‰V-PDB}) = (21.9 - 3.16 * (31.061 + T(\text{°C}))/0.5) + \delta^{18}\text{O}_{\text{sw}}(\text{‰V-PDB}) \quad (4)$$

The calculated $\delta^{18}\text{O}_{\text{sw, ivo}}$ were converted from V-PDB into Vienna Standard Mean Ocean Water (V-SMOW) scale according to equation of ref. 47:

$$\delta^{18}\text{O}(\text{‰V-PDB}) = 0.9998 * \delta^{18}\text{O}_{\text{sw}}(\text{‰V-SMOW}) - 0.27\text{‰} \quad (5)$$

Low (high) values of $\delta^{18}\text{O}_{\text{sw, ivo}}$ pointing to fresh (saline) ocean conditions. We performed an error propagation analysis to assess the error of the $\delta^{18}\text{O}_{\text{sw, ivo}}$ calculations considering the uncertainty in performed Mg/Ca and $\delta^{18}\text{O}$ measurements, the uncertainty of applied Mg/Ca calibration as well as the error involved in the relationship between salinity and $\delta^{18}\text{O}_{\text{sw}}$. We obtained an error of ~0.38 for reconstructions of $\delta^{18}\text{O}_{\text{sw, ivo}}$. A previous study reported similar error propagations for $\delta^{18}\text{O}_{\text{sw}}$ of 0.36 (+/–0.02‰) derived from $\delta^{18}\text{O}_{\text{calcite}}$ and Mg/Ca-temperature reconstructions of *N. pachyderma* sin. in the subpolar Pacific⁴⁸.

X-ray fluorescence scanning. X-ray fluorescence core-scanning measurements of GeoB18530-1 were performed with an Avaatech XRF Core Scanner at the MARUM, University of Bremen. Elemental intensities were obtained at 1 cm resolution over a 1.2 cm² area from the split core surface of the archive halves. The

split-core surface was scanned three times with different settings for light (e.g., Al, Ca; 10 kV, 20 s, 150 mA), medium (e.g. Sr, 30 kV, 20 s, 150 mA) and heavy (e.g. Ba; 50 kV, 20 s, 800 mA) elements. To avoid contamination of the XRF measurement unit the core surface was covered with a 4 µm thin SPEXcerti Prep Ultralene foil. The core scanner unit includes a Canberra X-PIPS Silicon Drift Detector (SDD; Model SXD 15C-150-500) with 150 eV X-ray resolution, a Canberra Digital Spectrum Analyser DAS 1000 and an Oxford Instruments 100 W Neptune X-ray tube with rhodium (Rh) target material. Raw data spectra were processed by Analysis of X-ray spectra by the Iterative Least square software (WIN AXIL) package from Canberra Eurisys.

Age models. The age model for gravity core GeoB18530-1 is based on 20 accelerator mass spectrometry radiocarbon dates from samples of *N. pachyderma* sin. (19 samples) and one mixed sample (*Globigerina bulloides* and *N. pachyderma* sin.) from core GeoB18530-1 (Supplementary Table 1). Radiocarbon ages were measured at Poznań Radiocarbon Laboratory as well as Physics Institute, University of Bern Climate and Environmental Physics Radiocarbon lab. The age model is based on an ensemble of 2,000 age-depth realizations calculated with the age modelling software BACON⁴⁹. Radiocarbon ages were calibrated using the IntCal20 calibration curve⁵⁰ and modelled local reservoir ages⁵¹ provided through the toolbox PaleoDataView⁵². To assess the uncertainty of Mg/Ca temperatures, we combined 2000 noisy proxy realisations with the 2000 BACON age models, interpolated the resulting 2000 time series to the median ages of all sampling depths and calculated the 95% confidence envelope for the Mg/Ca SSTs. We further re-calibrated the reported radiocarbon ages from site MD01-2461²⁴ following the same procedure as described for core GeoB18530-1.

Data availability

All relevant data in this paper are available at PANGAEA Data Publisher (<https://doi.org/10.1594/PANGAEA.943563>).

Received: 9 September 2021; Accepted: 28 June 2022;

Published online: 21 July 2022

References

- Heinrich, H. Origin and consequences of cyclic ice rafting in the northeast Atlantic Ocean during the past 130,000 years. *Quat. Res.* **29**, 142–152 (1988).
- Broecker, W. S., Bond, G., Klas, M., Clark, E. & McManus, J. Origin of the northern Atlantic's Heinrich events*. *Clim. Dyn.* **6**, 265–273 (1992).
- Bond, G. C. et al. Evidence for massive discharges of icebergs into the North Atlantic Ocean during the last glacial period. *Nature* **360**, 245–249 (1992).
- Bard, E., Rostek, F., Turon, J. L. & Gendreau, S. Hydrological impact of Heinrich Events in the subtropical northeast Atlantic. *Science* **289**, 1321–1324, <https://doi.org/10.1126/science.289.5483.1321> (2000).
- Voelker, A. H. L. et al. Global distribution of centennial-scale records for marine isotope stage (MIS) 3: a database. *Quat. Sci. Rev.* **21**, 1185–1214, [https://doi.org/10.1016/S0277-3791\(01\)00139-1](https://doi.org/10.1016/S0277-3791(01)00139-1) (2002).
- McManus, J., Francois, R., Gherardi, J., Keigwin, L. & Brown-Leger, S. Collapse and rapid resumption of Atlantic meridional circulation linked to deglacial climate change. *Nature* **428**, 834–837 (2004).
- MacAyeal, D. R. Binge/purge oscillations of the Laurentide Ice Sheet as a cause of the North Atlantic's Heinrich events. *Paleoceanography* **8**, 775–784, <https://doi.org/10.1029/93PA02200> (1993).
- Hulbe, C., MacAyeal, D., Denton, G., Kleman, J. & Lowell, T. Catastrophic ice shelf breakup as the source of Heinrich event icebergs. *Paleoceanography* **19**, PA1004, <https://doi.org/10.1029/2003PA000890> (2004).
- Álvarez-Solas, J. et al. Heinrich event 1: an example of dynamical ice-sheet reaction to oceanic changes. *Clim. Past* **7**, 1297–1306, <https://doi.org/10.5194/cp-7-1297-2011> (2011).
- Barker, S. et al. Icebergs not the trigger for North Atlantic cold events. *Nature* **520**, 333–336, <https://doi.org/10.1038/nature14330> (2015).
- Bassil, J. N., Petersen, S. V. & Cathles, L. M. Heinrich events triggered by ocean forcing and modulated by isostatic adjustment. *Nature* **542**, 332–334, <https://doi.org/10.1038/nature21069> (2017).
- Shaffer, G., Olsen, S. M. & Bjerrum, C. J. Ocean subsurface warming as a mechanism for coupling Dansgaard-Oeschger climate cycles and ice-rafting events. *Geophys. Res. Lett.* **31**, L24202, <https://doi.org/10.1029/2004GL020968> (2004).
- Álvarez-Solas, J. et al. Links between ocean temperature and iceberg discharge during Heinrich events. *Nat. Geosci.* **3**, 122–126, <https://doi.org/10.1038/NGEO752> (2010).
- Marcott, S. A. et al. Ice-shelf collapse from subsurface warming as a trigger for Heinrich events. *Proc. Natl Acad. Sci. USA* **108**, 13415–13419, <https://doi.org/10.1073/pnas.111657510> (2011).
- Hátún, H., Sando, A. B., Drange, H., Hansen, B. & Valdimarsson, H. Influence of the Atlantic subpolar gyre on the thermohaline circulation. *Science* **309**, 1841–1844, <https://doi.org/10.1126/science.11147> (2005).
- Ruddiman, W. F. Late Quaternary deposition of ice-rafted sand in the subpolar North Atlantic (lat 40° to 65°N). *Geol. Soc. Am. Bull.* **88**, 1813–1827 (1977).
- Mulitza, S. et al. T. RV MARIA S. MERIAN, Cruise 39, St. John's – St. John's, 07.06. – 25.06.2014, MARIA S. MERIAN-Berichte, MSM39. DFG-Senatskommission für Ozeanographie, p. 89, https://doi.org/10.2312/cr_msm39 (2015).
- Hodell, D. A., Channell, J. E. T., Curtis, J. H., Romero, O. E. & Röhl, U. Onset of “Hudson Strait” Heinrich events in the eastern North Atlantic at the end of the middle Pleistocene transition (~640 ka)? *Paleoceanography* **23**, PA4218, <https://doi.org/10.1029/2008PA001591> (2008).
- Channell, J. E. et al. A 750-kyr detrital-layer stratigraphy for the North Atlantic (IODP sites U1302–U1303, Orphan Knoll, Labrador Sea). *Earth Planet. Sci. Lett.* **317**, 218–230, <https://doi.org/10.1016/j.epsl.2011.11.029> (2012).
- Locarnini, R. A. et al. In *World Ocean Atlas 2013, Volume 1: Temperature*. (ed. Levitus, S) NOAA Atlas NESDIS, pp. 40, <https://doi.org/10.7289/V55X26VD> (2013).
- Hodell, D. A. et al. Anatomy of Heinrich Layer 1 and its role in the last deglaciation. *Paleoceanography* **32**, 284–303, <https://doi.org/10.1002/2016PA003028> (2017).
- North Greenland Ice Core Project members. et al. High-resolution record of Northern Hemisphere climate extending into the last interglacial period. *Nature* **431**, 147–151 (2004).
- Rasmussen, S. O. et al. A new Greenland ice core chronology for the last glacial termination. *J. Geophys. Res.* **111**, D06102, <https://doi.org/10.1029/2005JD006079> (2006).
- Peck, V. L., Hall, I. R., Zahn, R. & Elderfield, H. Millennial-scale surface and subsurface paleothermometry from the northeast Atlantic, 55–8 ka BP. *Paleoceanography* **23**, PA3221, <https://doi.org/10.1029/2008PA001631> (2008).
- Clark, C. D., Hughes, A. L., Greenwood, S. L., Jordan, C. & Sejrup, H. P. Pattern and timing of retreat of the last British-Irish Ice Sheet. *Quat. Sci. Rev.* **44**, 112–146, <https://doi.org/10.1016/j.quascirev.2010.07.019> (2012).
- Lippold, J. et al. Does sedimentary ²³¹Pa/²³⁰Th from the Bermuda Rise monitor past Atlantic Meridional Overturning Circulation? *Geophys. Res. Lett.* **36**, L12601, <https://doi.org/10.1029/2009GL038068> (2009).
- Carlson, A. E. et al. Geochemical proxies of North American freshwater routing during the Younger Dryas cold event. *Proc. Natl Acad. Sci. USA* **104**, 6556–6561, <https://doi.org/10.1073/pnas.0611313104> (2007).
- Murton, J., Bateman, M., Dallimore, S. R., Teller, J. T. & Yang, Z. Identification of Younger Dryas outburst flood path from Lake Agassiz to the Arctic Ocean. *Nature* **464**, 740–743, <https://doi.org/10.1038/nature08954> (2010).
- Rühlemann, C. et al. Intermediate depth warming in the tropical Atlantic related to weakened thermohaline circulation: combining paleoclimate data and modeling results for the last deglaciation. *Paleoceanography* **19**, PA1025, <https://doi.org/10.1029/2003PA000948> (2004).
- Pedro, J. B. et al. Beyond the bipolar seesaw: toward a process understanding of interhemispheric coupling. *Quat. Sci. Rev.* **192**, 27–46, <https://doi.org/10.1016/j.quascirev.2018.05.005> (2018).
- He, C. et al. North Atlantic subsurface temperature response controlled by effective freshwater input in “Heinrich” events. *Earth Planet. Sci. Lett.* **539**, 116247, <https://doi.org/10.1016/j.epsl.2020.116247> (2020).
- Álvarez-Solas, J., Robinson, A., Montoya, M. & Ritz, C. Iceberg discharges of the last glacial period driven by oceanic circulation changes. *Proc. Natl Acad. Sci. USA* **110**, 16350–16354, <https://doi.org/10.1073/pnas.130662211> (2013).
- Holland, D. M., Thomas, R. H., de Young, B., Ribergaard, M. H. & Lyberth, B. Acceleration of Jakobshavn Isbræ triggered by warm subsurface ocean waters. *Nat. Geosci.* **1**, 659–664, <https://doi.org/10.1038/ngeo316> (2008).
- Rignot, E., Koppes, M. & Velicogna, I. Rapid submarine melting of the calving faces of West Greenland glaciers. *Nat. Geosci.* **3**, 187–191, <https://doi.org/10.1038/NGEO765> (2010).
- Straneo, F. & Heimbach, P. North Atlantic warming and the retreat of Greenland's outlet glaciers. *Nature* **504**, 36–43, <https://doi.org/10.1038/nature12854> (2013).
- IPCC. Climate Change 2021: The Physical Science Basis. Contribution of Working Group I to the Sixth Assessment Report of the Intergovernmental Panel on Climate Change. (eds Masson-Delmotte, V. et al.) (Cambridge University Press, In Press, 2021).
- Boers, N. Observation-based early-warning signals for a collapse of the Atlantic Meridional Overturning Circulation. *Nat. Clim. Chang.* **11**, 680–688, <https://doi.org/10.1038/s41558-021-01097-4> (2021).

38. Barker, S., Greaves, M. & Elderfield, H. A study of cleaning procedures used for foraminiferal Mg/Ca paleothermometry. *Geochem. Geophys. Geosyst.* **4**, 8407, <https://doi.org/10.1029/2003GC000559> (2003).
39. Greaves, M. et al. Interlaboratory comparison study of calibration standards for foraminiferal Mg/Ca thermometry. *Geochem. Geophys. Geosyst.* **9**, <https://doi.org/10.1029/2008GC001974> (2008).
40. Simstich, J., Sarnthein, M. & Erlenkeuser, H. Paired d18O signals of *Neogloboquadrina pachyderma* (s) and *Turborotalita quinqueloba* show thermal stratification structure in Nordic seas. *Mar. Micropaleontol.* **48**, 107–125, [https://doi.org/10.1016/S0377-8398\(02\)00165-2](https://doi.org/10.1016/S0377-8398(02)00165-2) (2003).
41. Mashiotta, T. A., Lea, D. W. & Spero, H. J. Glacial-interglacial changes in Subantarctic sea surface temperature and d18O water using foraminiferal Mg. *Earth Planet. Sci. Lett.* **170**, 417–432, [https://doi.org/10.1016/S0012-821X\(99\)00116-8](https://doi.org/10.1016/S0012-821X(99)00116-8) (1999).
42. Kozdon, R., Eisenhauer, A., Weinelt, M., Meland, M. Y. & Nuernberg, D. Reassessing Mg/Ca temperature calibrations of *Neogloboquadrina pachyderma* (sinistral) using paired d44/40Ca and Mg/Ca measurements. *Geochem. Geophys. Geosyst.* **10**, Q03005, <https://doi.org/10.1029/2008GC002169> (2009).
43. Ezat, M. M., Rasmussen, T. L. & Groeneveld, J. Reconstruction of hydrographic changes in the southern Norwegian Sea during the past 135 kyr and the impact of different foraminiferal Mg/Ca cleaning protocols. *Geochem. Geophys. Geosyst.* **17**, 3420–3436, <https://doi.org/10.1002/2016GC006325> (2016).
44. Kretschmer, K., Kucera, M. & Schulz, M. Modeling the distribution and seasonality of *Neogloboquadrina pachyderma* in the North Atlantic Ocean during Heinrich Stadial 1. *Paleoceanography* **31**, 986–1010, <https://doi.org/10.1002/2015PA002819> (2016).
45. Waelbroeck, C., Labeyrie, L., Michel, E., Duplessy, J. C. & McManus, J. Sea-level and deep water temperature changes derived from benthic foraminifera isotopic records. *Quat. Sci. Rev.* **21**, 295–305, [https://doi.org/10.1016/S0277-3791\(01\)00101-9](https://doi.org/10.1016/S0277-3791(01)00101-9) (2002).
46. Shackleton, N. J. Attainment of isotopic equilibrium between ocean water and the benthonic foraminifera genus *Uvigerina*: Isotopic changes in the ocean during the last glacial. *Colloques Internationaux du C.N.R. S. 219 – Les Méthodes Quantitatives D'étude des Variations du Climat au Cours du Pléistocène*, 203–209 (1974).
47. Hut, G. Consultants' Group Meeting on Stable Isotope Reference Samples for Geochemical and Hydrological Investigations, Rep. to Dir. Gen., Vienna, 16–18 September 1985, Int. At. Energy Agency, Vienna, p. 428 (1987).
48. Riethdorf, J. R., Max, L., Nürnberg, D., Lembke-Jene, L. & Tiedemann, R. Deglacial development of (sub) sea surface temperature and salinity in the subarctic northwest Pacific: Implications for upper-ocean stratification. *Paleoceanography* **28**, 91–104, <https://doi.org/10.1002/palo.20014> (2013).
49. Blaauw, M. & Christen, J. A. Flexible paleoclimate age-depth models using an autoregressive gamma process. *Bayesian Anal.* **6**, 457–474 (2011).
50. Reimer, P. et al. The IntCal20 northern hemisphere radiocarbon age calibration curve (0–55 cal kBP). *Radiocarbon* **62**, 725–757, <https://doi.org/10.1017/RDC.2020.41> (2020).
51. Butzin, M., Heaton, T., Köhler, P. & Lohmann, G. A short note on marine reservoir age simulations used in IntCal20. *Radiocarbon* **62**, 865–871, <https://doi.org/10.1017/RDC.2020.9> (2020).
52. Langner, M. & Mulitza, S. Technical Note: PaleoDataView – A software toolbox for the collection, homogenization and visualization of marine proxy data. *Clim. Past* **15**, 2067–2072, <https://doi.org/10.5194/cp-15-2067-2019> (2019).
53. Dyke, A. S. et al. The Laurentide and Innuitian ice sheets during the Last Glacial Maximum. *Quat. Sci. Rev.* **21**, 9–31, [https://doi.org/10.1016/S0277-3791\(01\)00095-6](https://doi.org/10.1016/S0277-3791(01)00095-6) (2002).
54. Schlitzer, R. Data analysis and visualization with ocean data view. *CMOS Bull. SCMO* **43**, 9e13 (2015).

Acknowledgements

Sample material has been provided by the GeoB Core Repository at the MARUM - Center for Marine Environmental Sciences, University of Bremen. This research used data acquired at the Core Scanner Lab at MARUM - Center for Marine Environmental Sciences, University of Bremen. We thank V. Lukies for the technical support in the Core Scanner Lab. N. Gehre is acknowledged for lab support and preparation of Mg/Ca and stable isotope measurements. L.M. wishes to extend his special thanks to C. Kricke, H. Max and L. Max for their continuous and unparalleled patience and support. L.M. received financial support from the Deutsche Forschungsgemeinschaft (DFG) through grant 47010623 (SAINT). C.M.C. acknowledges the financial support from FAPESP (grants 2018/15123-4 and 2019/24349-9), CAPES (grant 88881.313535/2019-01), CNPq (grant 312458/2020-7) and the Alexander von Humboldt Foundation.

Author contributions

L.M. and S.M. designed the study, L.M. collected the XRF data, L.M. and S.M. provided radiocarbon data, L.M. and M.M.L. prepared and analysed $\delta^{18}\text{O}$ data, D.N. facilitated Mg/Ca measurements and additional stable isotope measurements. C.M.C. contributed to sample collection and background knowledge. L.M., D.N., C.M.C. and S.M. wrote the first draft of the manuscript. All authors contributed to the interpretation and the preparation of the final manuscript.

Funding

Open Access funding enabled and organized by Projekt DEAL.

Competing interests

The authors declare no competing interests.

Additional information

Supplementary information The online version contains supplementary material available at <https://doi.org/10.1038/s41467-022-31754-x>.

Correspondence and requests for materials should be addressed to Lars Max.

Peer review information *Nature Communications* thanks Jorge Alvarez-Solas, Lev Tarasov and Jimin Yu for their contribution to the peer review of this work. Peer reviewer reports are available.

Reprints and permission information is available at <http://www.nature.com/reprints>

Publisher's note Springer Nature remains neutral with regard to jurisdictional claims in published maps and institutional affiliations.



Open Access This article is licensed under a Creative Commons Attribution 4.0 International License, which permits use, sharing, adaptation, distribution and reproduction in any medium or format, as long as you give appropriate credit to the original author(s) and the source, provide a link to the Creative Commons license, and indicate if changes were made. The images or other third party material in this article are included in the article's Creative Commons license, unless indicated otherwise in a credit line to the material. If material is not included in the article's Creative Commons license and your intended use is not permitted by statutory regulation or exceeds the permitted use, you will need to obtain permission directly from the copyright holder. To view a copy of this license, visit <http://creativecommons.org/licenses/by/4.0/>.

© The Author(s) 2022